http://www.jourmag.org/index.php/jma
Journal of Magnetism and Its Applications

Research articles

Parametric Optimisation of the SG6042 Airfoil for Improved Lift-to-Drag Performance of Small Horizontal Axis Wind Turbines at Low Reynolds Numbers

Muhammad Ramzan Luhur [1], Sher Muhammad Ghoto2, Aijaz Abbasi[3], Muhammad Kashif abbasi[4], Azhar Hussain shah[5] sajjad bhangwar[6] , Arif Ali Rind[7]
[1,2,3,5,6,7] Department of Mechanical Engineering
Quaid-e-Awam University of Engineering, Science and Technology, Nawabshah, Sindh, Pakistan
[4]Department of Industrial & Manufacturing Engineering, Quaid-e-Awam University of Engineering, Science and Technology, Nawabshah, Sindh, Pakistan
Corresponding author (luhur@quest.edu.pk)

Article info

Keywords:
low Reynolds number airfoil;
SG6042;
small horizontal axis wind turbine;
lift-to-drag ratio;
QBlade;
thickness-to-camber ratio

Abstract

Small horizontal axis wind turbines (HAWTs) operate at chord Reynolds numbers well below those of utility-scale machines, typically between 1×10^5 and 6×10^5, where laminar separation raises profile drag and lowers the lift-to-drag ratio of conventional airfoils. This study presents a numerical optimisation of the SG6042 airfoil, a section developed for small wind turbines, with the objective of raising its maximum lift-to-drag ratio (CL/CD) under low Reynolds number conditions. The baseline SG6042 geometry, with 10 percent thickness and 3.75 percent camber, was analysed in QBlade, which couples the XFOIL panel method with blade design routines, and the computed performance was compared with published wind tunnel data. Eighteen modified profiles were then generated by varying maximum thickness from 5 to 9 percent of chord and maximum camber from 5 to 9 percent of chord, and each profile was analysed at Reynolds numbers from 1×10^5 to 6×10^5 over an incremental sweep of angle of attack. All modified profiles outperformed the baseline. Peak efficiency moved to lower angles of attack as Reynolds number increased, from 5.5 to 6 degrees at Re = 1×10^5 to 3 to 3.5 degrees at Re = 5×10^5 and 6×10^5. The best three sections, SG6042M5-7, SG6042M5-8 and SG6042M5-9, combine 5 percent thickness with 7 to 9 percent camber and reached maximum CL/CD values of 178.25, 182.41 and 182.40 respectively at 3.5 degrees and Re = 5×10^5, against 124.10 for the baseline under identical computational settings, an improvement of about 47 percent. The results confirm that reduced thickness combined with raised camber is an effective route to high aerodynamic efficiency for small HAWT blades, subject to structural verification and experimental validation.

1. Introduction

1.1 Background

Wind energy occupies a central position among renewable resources because it can be deployed at scales ranging from a few hundred watts to several megawatts. The theoretical ceiling on the energy that a turbine rotor can extract from the wind is fixed by the Betz limit at 59.3 percent of the kinetic energy flux through the rotor disc (Betz, 1966). Within this ceiling, the actual power coefficient of a machine is governed largely by the aerodynamic quality of its blades, and the aerodynamic quality of a blade depends in the first instance on the airfoil sections from which it is built.Small horizontal axis wind turbines (HAWTs), generally taken as machines with rated power below about 50 kW, are attractive for distributed and off-grid generation in rural and peri-urban areas. Their blades, however, operate under conditions that differ sharply from those of utility-scale rotors. Because chord lengths are short and tip speeds moderate, the chord Reynolds number of a small HAWT blade typically lies between 1×10^4 and 6×10^5 (Miley, 1982). In this regime the boundary layer over much of the blade remains laminar, and a laminar boundary layer separates readily under the adverse pressure gradient on the rear portion of the suction surface. The separated shear layer may undergo transition and reattach, forming a laminar separation bubble. The bubble thickens the boundary layer, raises the profile drag and, in unfavourable cases, bursts with a sudden loss of lift. The practical consequence is that airfoils designed for chord Reynolds numbers of several million perform poorly on small machines, and the lift-to-drag ratio CL/CD, the single most useful indicator of section efficiency, falls well below the values achieved at high Reynolds numbers (Giguère & Selig, 1997).The selection and refinement of the airfoil section is therefore the first-order design decision for a small HAWT. Once a section with a high lift-to-drag ratio in the operating Reynolds number range has been fixed, the chord and twist distributions along the span follow from blade element momentum analysis. Panel-method codes are the standard tools at this stage of design. XFOIL combines a linear-vorticity panel method with an integral boundary layer formulation and an e^N transition criterion, and it predicts low Reynolds number section behaviour at a small fraction of the cost of Navier-Stokes computation (Drela, 1989). QBlade wraps the XFOIL routines inside an open-source blade design environment and has been applied widely in small wind turbine studies (Alaskari, Abdullah, & Majeed, 2019).

1.2 Research gap

Giguère and Selig (1998) developed the SG604x family specifically for small wind turbines and measured maximum lift-to-drag ratios of 87, 84, 106 and 125 for the SG6040, SG6041, SG6042 and SG6043 respectively at Re = 5×10^5, with thickness emerging as the principal penalty on peak performance. The SG6042, with a maximum thickness of 10 percent of chord and a maximum camber of 3.75 percent, offers a workable compromise between aerodynamic performance and the structural depth required near the blade root, and it has been adopted in a number of small rotor designs. Later work has produced several purpose-designed low Reynolds number sections, reviewed in Section 2, yet the published record contains few studies that isolate, in a systematic manner, the joint effect of maximum thickness and maximum camber on the SG6042 across the full Reynolds number range in which small machines operate. Parametric studies of thickness and camber exist for NACA four-digit sections (Roy, Das, & Biswas, 2021; Davari et al., 2023), but comparable data for the SG family are scarce, and the movement of the optimal angle of attack with Reynolds number has not been mapped for modified SG6042 geometries. The present work addresses this gap.

1.3 Aim and objectives

The aim of this study is to optimise the design of the SG6042 airfoil so as to contribute an efficient low Reynolds number section for small horizontal axis wind turbines. Two objectives follow from this aim. The first is to select the SG6042 airfoil and verify its reported performance through panel-method analysis in QBlade. The second is to modify and optimise the SG6042 geometry on the basis of changes in the thickness-to-camber ratio, the angle of attack and the Reynolds number, and to identify the modified sections that yield the highest lift-to-drag ratio.

1.4 Significance of the study

A higher section lift-to-drag ratio translates directly into a higher rotor power coefficient and better energy capture at sites with low mean wind speeds, which are precisely the sites where small machines are installed. The case for such machines is strongest in developing countries, where dispersed rural settlements lie far from the grid and the cost of grid extension exceeds the cost of local generation; in such settings a small rotor that extracts even a few percent more energy from the same wind resource changes the economics of the installation. The parametric maps produced here can be carried straight into blade element momentum design, since they report the optimal angle of attack at each Reynolds number, and hence the local incidence that the twist schedule of a blade should maintain along its span. The remainder of the paper is organised as follows. Section 2 reviews the relevant literature. Section 3 sets out the computational method and the parametric modification programme. Section 4 presents and discusses the results, and Section 5 records the conclusions and the work that remains.

2. Literature Review

2.1 Wind tunnel investigations of low Reynolds number airfoils

Systematic measurement campaigns, above all those conducted at the University of Illinois, established the empirical base for low Reynolds number wind turbine aerodynamics. Giguère and Selig (1998) designed and tested the SG6040 to SG6043 family for small HAWTs and reported maximum lift-to-drag ratios of 87, 84, 106 and 125 at Re = 5×10^5, with the thinner members of the family performing best: the 16 percent thick SG6040 lagged the 10 percent thick SG6042 and SG6043 by a wide margin. An earlier survey by the same authors set out the general requirements for small turbine sections, including soft stall behaviour and low sensitivity to leading edge roughness (Giguère & Selig, 1997). Selig and McGranahan (2004) measured six candidate sections, the E387, FX 63-137, S822, S834, SD2030 and SH3055, at Reynolds numbers from 1×10^5 to 5×10^5 and documented the sharp rise of drag with angle of attack at the lower end of the range, where the laminar separation bubble dominates the drag budget. Rasheed and Al-Qaisy (2008) examined the NACA 23015 in a subsonic wind tunnel and recorded large changes in pressure and lift coefficients between effective angles of 9 and 15 degrees, which illustrates the sensitivity of moderately thick sections near stall. Miley's (1982) catalogue of low Reynolds number airfoil data remains a standard reference for the regime below Re = 5×10^5 and documents the general degradation of section performance as Reynolds number falls.

2.2 Purpose-designed low Reynolds number sections

A second line of work has produced sections designed from the outset for the low Reynolds number regime. Singh, Ahmed, Zullah and Lee (2012) developed the AF300, a thick cambered section intended to improve the starting behaviour of small rotors at wind speeds below 4 m/s, and confirmed its performance through wind tunnel tests; a companion study validated the resulting blade through two-dimensional computation and rotor testing (Singh & Ahmed, 2013). Shah, Bhattarai, Mathew and Lim (2012) reported the UBD6166 section with a maximum lift-to-drag ratio of 66.9 at Re = 1×10^5, and the same group later presented the UBD54-94 profile, which holds its best efficiency near the design lift coefficient over Reynolds numbers from 3×10^4 to 1×10^5 and is suited to blade tip stations (Shah, Mathew, & Lim, 2014). Henriques, Marques da Silva, Estanqueiro and Gato (2009) applied a pressure-load inverse method to obtain the T.Urban 10/193 section for turbines in the built environment, achieving a lift-to-drag ratio of 95 at Re = 5×10^5 with a stall angle of 12 degrees. Bio-inspired design has also been attempted: a section derived from the seagull wing produced maximum lift-to-drag ratios of 38, 52 and 57 at Re = 1×10^5, 3.5×10^5 and 6×10^5 respectively (Limin et al., 2011). Wata et al. (2011) blended the SG6043 with the Eppler 422 to form a hybrid profile that reached a maximum lift-to-drag ratio of 80 at Re = 2.05×10^5. Leloudas et al. (2020) generated a family of sections from the RG15 with graded thickness for different span stations, accepting a reduction in the maximum lift-to-drag ratio of the thicker members in exchange for structural depth and better starting response. The consistent message of this body of work is that thickness purchases structural capacity at a direct cost in peak aerodynamic efficiency.

2.3 Computational studies with panel methods and CFD

Panel methods and Reynolds-averaged Navier-Stokes (RANS) computation have both been applied to section selection for small machines. Hossain, Raiyan, Akanda and Jony (2014) compared the NACA 6409 and NACA 4412 numerically and found the more moderately cambered NACA 4412 superior in lift-to-drag ratio over the angles examined. Suresh and Rajakumar (2019) screened ten candidate sections in QBlade for a low wind speed rural application and identified the SD7080 as the most suitable. Noronha and Krishna (2020) designed a micro HAWT in MATLAB and QBlade with the SG6040 and SG6041 as hub and tip sections and interpolated intermediate profiles between them. Khalil, Tenghiri, Abdi and Bentamy (2020) coupled a blade geometry optimiser to section data and obtained a peak power coefficient of 0.42 for an 11 kW rotor built on the FX 63-137. Alaskari, Abdullah and Majeed (2019) analysed the SG6043 in QBlade and located its maximum lift-to-drag ratio at an angle of attack of 2 degrees. Osei, Opoku, Sunnu and Adaramola (2020) used XFOIL to develop three high-performance sections for small wind turbines and reported maximum lift-to-drag ratios of 134, 131 and 127 at Re = 3×10^5.RANS studies supply a check on panel-method output. Yao et al. (2012) computed two-dimensional wind turbine sections at Re = 5×10^5 across a wide range of angles of attack. Yang, Chang and Arici (1995) computed the NREL S809 with a k-omega closure and recorded discrepancies against measured lift and drag near stall, a reminder that turbulence modelling near separation remains the weak point of two-dimensional RANS. Jha et al. (2018) documented the Reynolds number dependence of the NACA 0012, with a stronger lift response at Re = 2.21×10^5 and a reduced lift-to-drag ratio at higher Reynolds numbers. Related CFD work on vertical axis machines (Castelli, Englaro, & Benini, 2011; Y. Wang et al., 2018), on section comparisons at fixed relative thickness (J. Wang et al., 2011) and on the widely used NACA 4412 (Kevadiya & Vaidya, 2013) completes the computational picture.

2.4 Thickness and camber as design variables

The geometric parameters most directly tied to peak efficiency are maximum camber, maximum thickness and their ratio. Roy, Das and Biswas (2021) varied camber ratio and thickness ratio across NACA four-digit sections at Re = 3.6×10^5 and showed that camber governs the level of the lift curve while thickness mainly conditions drag and stall character. Davari et al. (2023) treated the thickness-to-camber ratio as the primary design variable and demonstrated that the peak lift-to-drag ratio of a section can be maximised by direct adjustment of this ratio. Alsahlani, Al-Saad and Al-Mosallam (2023) compared NACA, PARSEC and Bezier curve parameterisations under low Reynolds number conditions and confirmed that modest geometric changes produce large movements in section efficiency in this regime.

2.5 Summary of the literature and the gap

Taken together, the literature establishes three points. First, the peak lift-to-drag ratio in the low Reynolds number regime is strongly conditioned by section geometry, and thin, well-cambered profiles outperform thick ones. Second, panel-method tools of the XFOIL class are accepted instruments for parametric section studies in this regime, provided their known tendency to overpredict performance is kept in view. Third, while parametric thickness and camber studies exist for NACA sections, no published study has mapped the joint effect of thickness and camber on the SG6042 across Reynolds numbers from 1×10^5 to 6×10^5, nor reported how the optimal angle of attack of modified SG6042 geometries moves with Reynolds number. Most reported optimisation studies also stop short of experimental confirmation of the optimised geometry. The present study supplies the missing parametric mapping and identifies the resulting optimal sections, while leaving experimental confirmation to future work.

3. Research Methodology

3.1 Overall procedure

The study followed a seven-step procedure, summarised in Figure 1. A literature survey identified candidate sections and fixed the selection criteria; the SG6042 was selected as the base airfoil; its baseline performance was computed in QBlade and compared with published data; a matrix of modified geometries was generated by varying thickness and camber; each geometry was analysed over sweeps of angle of attack and Reynolds number; the profiles exceeding a lift-to-drag threshold were shortlisted; and the best sections were compared with the baseline and with published results. The steps are described in turn below.

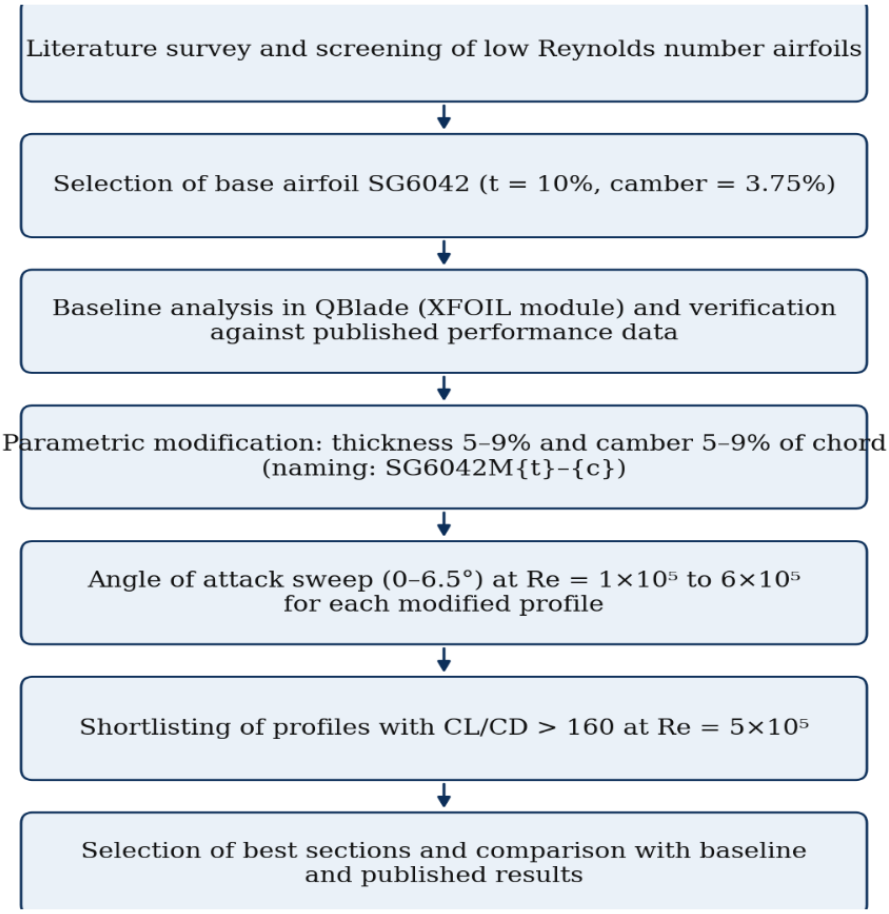


Figure 1Flowchart of the research methodology

3.2 Selection of the base airfoil

The selection criteria were a high lift coefficient at low Reynolds numbers, a low drag coefficient, stable behaviour in the low-speed regime, a documented wind tunnel pedigree against which computed results could be checked, and an established record of use on small wind turbine blades. The SG6042 satisfies all five criteria. It belongs to a family designed expressly for small HAWTs, its measured polars are available in the open literature (Giguère & Selig, 1998), and at Re = 5×10^5 it delivers a measured maximum lift-to-drag ratio of 106, second in its family only to the thinner SG6043. The baseline geometry has a maximum thickness of 10 percent of chord, a maximum camber of 3.75 percent of chord and a thickness-to-camber ratio of 2.66. Published coordinates of the section were used throughout.

3.3 Computational tool and settings

All aerodynamic analyses were performed in QBlade, whose two-dimensional module embeds the XFOIL viscous panel code (Drela, 1989). The SG6042 coordinates were imported, the Reynolds number was set in steps of 1×10^5 from 1×10^5 to 6×10^5, and the angle of attack was swept incrementally for each Reynolds number. The lift coefficient, drag coefficient and lift-to-drag ratio were extracted at intervals of 0.5 degrees, and results are reported here over the window of 3 to 6 degrees within which the efficiency peaks of all geometries fall. The transition and convergence settings of the XFOIL module were kept at their default values, and the same settings were applied to every geometry so that all comparisons rest on an identical computational basis.

3.4 Verification of the baseline

The computed baseline performance was compared with the wind tunnel measurements of Giguère and Selig (1998). The computation places the peak lift-to-drag ratio of the SG6042 at 124.18 at an angle of attack of 3.5 degrees and Re = 5×10^5, against a measured maximum of 106 at the same Reynolds number. An overprediction of this order is a known property of panel methods at low Reynolds numbers, which tend to underestimate the drag contribution of the laminar separation bubble. The position of the peak and the shape of the computed curves agree with the measured behaviour, and the ordering of sections by efficiency is preserved. For this reason the study draws its conclusions from relative comparisons among geometries analysed under identical settings, rather than from absolute values.

3.5 Parametric modification programme

Modified geometries were generated by scaling the thickness and camber distributions of the parent section. Maximum thickness was varied from 5 to 9 percent of chord and maximum camber from 5 to 9 percent of chord, each in steps of 1 percent, with one parameter changed at a time so that individual effects could be separated. Each variant is denoted SG6042M{t}-{c}, where t and c are the maximum thickness and maximum camber in percent of chord; SG6042M5-8, for example, carries 5 percent thickness and 8 percent camber. The eighteen variants carried into the full analysis are listed in Table 1 together with their thickness-to-camber ratios, which range from 0.555 to 1.285 against 2.66 for the baseline. For every variant the full sweep of angle of attack was repeated at each of the six Reynolds numbers.

Table 1 Baseline geometry and parametric modification matrix of the SG6042 airfoil

Airfoil	Thickness (% chord)	Camber (% chord)	Thickness-to-camber ratio
SG6042 (baseline)	10.00	3.75	2.66
SG6042M5-5	5.00	5.00	1.000
SG6042M5-6	5.00	6.00	0.833
SG6042M5-7	5.00	7.00	0.714
SG6042M5-8	5.00	8.00	0.625
SG6042M5-9	5.00	9.00	0.555
SG6042M6-5	6.00	5.00	1.200
SG6042M6-6	6.00	6.00	1.000
SG6042M6-7	6.00	7.00	0.857
SG6042M6-8	6.00	8.00	0.750
SG6042M6-9	6.00	9.00	0.666
SG6042M7-7	7.00	7.00	1.000
SG6042M7-8	7.00	8.00	0.875
SG6042M7-9	7.00	9.00	0.778
SG6042M8-8	8.00	8.00	1.000
SG6042M8-9	8.00	9.00	0.888
SG6042M9-7	9.00	7.00	1.285
SG6042M9-8	9.00	8.00	1.125
SG6042M9-9	9.00	9.00	1.000

3.6 Shortlisting criterion

To reduce the eighteen variants to a manageable set of candidates, a threshold was applied: variants achieving a lift-to-drag ratio above 160 at Re = 5×10^5 were retained for detailed comparison. The shortlisted sections were then compared with the baseline and with one another over the full range of angle of attack and Reynolds number, and the best three were selected on the basis of peak lift-to-drag ratio and breadth of the efficiency plateau.

4. Results and Discussion

4.1 Baseline performance of the SG6042

Table 2 records the computed lift-to-drag ratio of the baseline SG6042 over angles of attack from 3 to 6 degrees at the six Reynolds numbers, and Figure 2 plots the same data. Two features stand out. First, the absolute level of efficiency rises steadily with Reynolds number: the peak climbs from 63.07 at Re = 1×10^5 to 124.18 at Re = 5×10^5 and 131.19 at Re = 6×10^5, a doubling across the operating range of a small machine. Second, the angle of attack at which the peak occurs falls as Reynolds number rises. At Re = 1×10^5 the efficiency is still increasing at 6 degrees, the upper edge of the reported window; at Re = 2×10^5 the peak sits near 5 degrees; by Re = 5×10^5 it has moved to 3.5 degrees and at Re = 6×10^5 to 3 degrees. The physical cause is the laminar separation bubble. At low Reynolds numbers the bubble is long, the drag penalty is large at all angles, and the most favourable operating point lies at higher incidence where the lift gain still outweighs the drag. As the Reynolds number rises, transition moves forward, the bubble shortens, the low-drag region of the polar widens at low incidence, and the lift-to-drag peak moves down the angle of attack axis.

Table 2 Computed lift-to-drag ratio of the baseline SG6042 airfoil

AoA (deg)	Re = 1×10^5	Re = 2×10^5	Re = 3×10^5	Re = 4×10^5	Re = 5×10^5	Re = 6×10^5
3.0	29.41	75.04	99.34	113.87	123.77	131.19
3.5	37.51	80.78	103.13	116.06	124.18	129.13
4.0	42.70	85.96	105.09	115.46	121.04	124.74
4.5	49.33	88.85	103.94	111.68	115.34	117.45
5.0	59.79	88.89	100.17	105.25	108.68	111.23
5.5	60.69	86.43	94.75	99.50	102.50	104.96
6.0	63.07	81.76	88.80	93.06	96.96	99.86

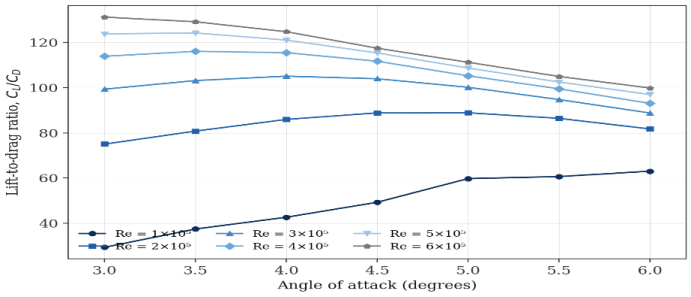


Figure 2 Lift-to-drag ratio of the baseline SG6042 versus angle of attack at six Reynolds numbers

The computed peak of 124.18 at Re = 5×10^5 exceeds the wind tunnel value of 106 reported by Giguère and Selig (1998) by about 17 percent, in line with the panel-method bias discussed in Section 3.4. The comparisons that follow are therefore made against the computed baseline, so that the reported gains are free of this bias.

4.2 Effect of camber at constant thickness

With thickness held at 5 percent of chord, raising the maximum camber from 7 to 9 percent moves the peak lift-to-drag ratio at Re = 5×10^5 from 178.25 for SG6042M5-7 to 182.41 for SG6042M5-8 and 182.40 for SG6042M5-9, in every case at an angle of attack of 3.5 degrees. The gain from 7 to 8 percent camber is about four points; the further step from 8 to 9 percent leaves the peak essentially unchanged. The benefit of the highest camber appears instead away from the peak: at 4 degrees SG6042M5-9 holds 181.0 against 177.85 for SG6042M5-8, and at 5 degrees it holds 160.0 against 153.30. Camber raises the lift coefficient at a given incidence, while its drag penalty grows as the suction-side pressure recovery steepens; the two effects balance near 8 to 9 percent camber, so the peak saturates, but the broader efficiency plateau of the 9 percent section gives it better tolerance of off-design operation. The same pattern, with lower absolute values, was observed at 5 and 6 percent camber: the computed polar of SG6042M5-5, the lowest camber variant at this thickness, peaks near 162 at Re = 5×10^5 and an angle of attack of 3 degrees, still well above the baseline but a full twenty points below the 8 and 9 percent camber variants. The discussion therefore concentrates on the 7 to 9 percent camber range, within which the shortlisted sections lie.

4.3 Effect of thickness at constant camber

Figure 3 shows the effect of thickness at a constant camber of 8 percent and Re = 5×10^5. The peak lift-to-drag ratio falls monotonically as thickness rises, from 182.41 at 5 percent thickness to 177.85, 172.70, 167.67 and 162.25 at 6, 7, 8 and 9 percent respectively, all peaks lying at 3.5 degrees. The same ordering holds at 9 percent camber, where the peak falls from 182.40 at 5 percent thickness to 161.80 at 9 percent. In round figures, each additional percent of thickness costs about five points of peak efficiency, or roughly 11 percent across the four-point thickness range examined. The mechanism is familiar: a thicker section imposes a steeper pressure recovery on the suction surface, which at low Reynolds numbers lengthens the laminar separation bubble and raises form drag. The result agrees with the ordering measured within the SG604x family by Giguère and Selig (1998) and with the thickness trade-off reported by Leloudas et al. (2020). Even the thickest variant examined, at 9 percent, remains well above the 10 percent thick baseline at every angle of attack, which shows that the camber increase carries the larger share of the overall gain.

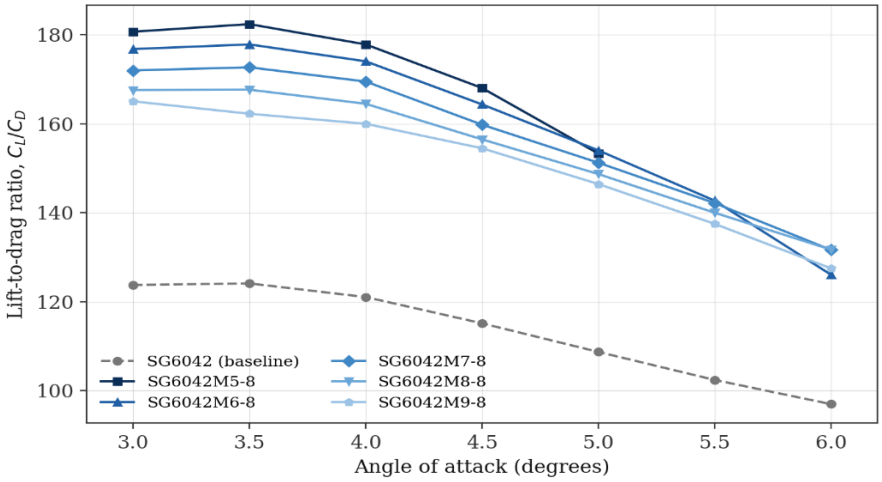


Figure 3 Effect of thickness on lift-to-drag ratio at a constant camber of 8 percent of chord, Re = 5×10^5.

4.4 Movement of the optimal angle of attack with Reynolds number

Across all modified profiles, the angle of attack at which the lift-to-drag ratio peaks falls steadily with Reynolds number: the best performance was observed at 5.5 to 6 degrees at Re = 1×10^5, at 5 to 5.5 degrees at Re = 2×10^5, at 4.5 to 5 degrees at Re = 3×10^5, at 4 to 4.5 degrees at Re = 4×10^5, and at 3 to 3.5 degrees at Re = 5×10^5 and 6×10^5. Figure 4 plots this band together with the optimum of the baseline section, which follows the same trend. At Re = 6×10^5 every modified profile delivered a lift-to-drag ratio above 160. The design implication is direct. The chord Reynolds number of a small HAWT blade varies along the span and with wind speed, so the local twist should be scheduled to hold each station near the band of Figure 4 rather than at a single fixed incidence. Inboard stations, which run at lower Reynolds numbers, should be set at higher local incidence than outboard stations. The band also warns against tuning a blade at a single test condition: a twist schedule fixed for Re = 5×10^5 will sit about two degrees below the optimum when the same station operates at Re = 1×10^5 in light winds.

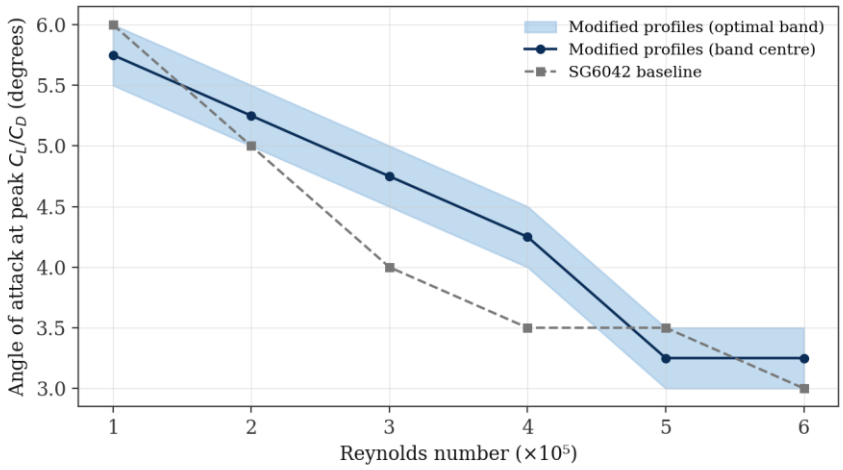


Figure 4 Angle of attack at peak lift-to-drag ratio versus Reynolds number for the modified profiles (band) and the baseline SG6042.

4.5 Selection of the optimal sections

Application of the shortlisting threshold of Section 3.6 retained the thin, highly cambered corner of the matrix, and three sections emerged as the best candidates: SG6042M5-7, SG6042M5-8 and SG6042M5-9. Figure 5 compares their geometries with the baseline; all three share the 5 percent thickness envelope and differ in the height of the camber line. Figure 6 plots their lift-to-drag curves against the baseline at Re = 5×10^5, and Table 3 summarises the peak values. SG6042M5-8 and SG6042M5-9 reach 182.41 and 182.40 respectively at 3.5 degrees, a gain of 47.0 percent over the computed baseline peak of 124.10, while SG6042M5-7 reaches 178.25, a gain of 43.6 percent. The difference between the top two sections at the peak is within the resolution of the method and should not be read as a ranking. Away from the peak the sections separate: SG6042M5-9 holds the highest values from 4 to 5.5 degrees and is the better choice where the operating incidence wanders, while SG6042M5-7, with the lowest camber of the three, will carry the smallest pitching moment and the mildest torsional load on the blade and may be preferred where structural simplicity matters. The pitching moment was not computed in this study and the structural remark is qualitative.

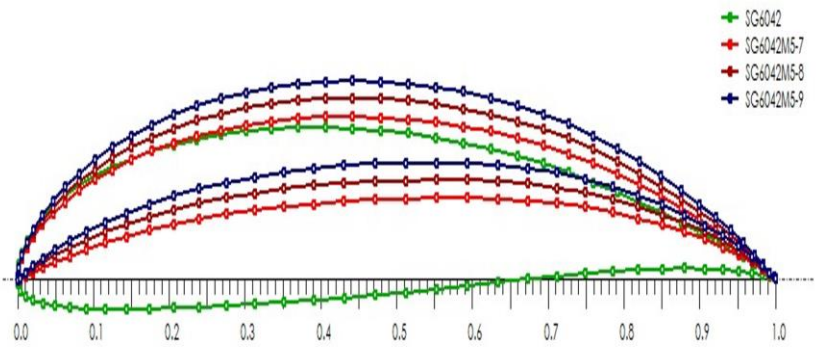


Figure 5 Profile geometries of the baseline SG6042 and the three best modified sections (adapted from the QBlade geometry module).

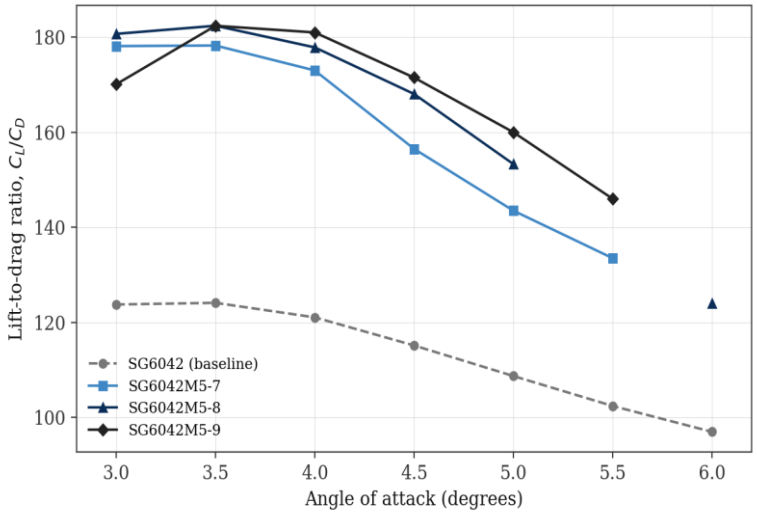


Figure 6 Lift-to-drag ratio of the three best modified sections and the baseline at Re = 5×10^5.

Table 3 Peak lift-to-drag performance of the best modified sections at Re = 5×10^5, compared with the baseline.

Airfoil	Thickness (%)	Camber (%)	t/c ratio	Peak CL/CD	AoA at peak (deg)	Gain over baseline (%)
SG6042 (baseline)	10.0	3.75	2.66	124.10	3.5	-
SG6042M5-7	5.0	7.0	0.714	178.25	3.5	43.6
SG6042M5-8	5.0	8.0	0.625	182.41	3.5	47.0
SG6042M5-9	5.0	9.0	0.555	182.40	3.5	47.0

4.6 Comparison with published results

The computed peaks of 178 to 182 sit well above the measured maximum of 125 for the SG6043, the best of the parent family (Giguère & Selig, 1998), and above the XFOIL-based maxima of 127 to 134 reported by Osei, Opoku, Sunnu and Adaramola (2020) at Re = 3×10^5. Part of this margin is genuine geometric improvement and part is the optimism of the panel method, which grows for thin, highly loaded sections where the real flow is most prone to separation. The defensible claim is therefore the relative one: under identical computational settings the best modified sections deliver about 47 percent more peak efficiency than the parent SG6042, and the parametric direction of the gain, namely less thickness and more camber, agrees with the wind tunnel record of the SG family and with the parametric findings of Roy, Das and Biswas (2021) and Davari et al. (2023) for NACA sections.

4.7 Limitations

Five limitations bound the present results. First, the analysis is two-dimensional and rests on a panel method with an integral boundary layer; absolute values of lift-to-drag ratio are overpredicted, as the baseline comparison in Section 3.4 shows, and the overprediction is likely larger for

the thin, highly cambered variants. Second, the default transition settings were used throughout, and no sensitivity study of the critical amplification factor or of leading edge roughness was performed; rough operating environments are known to erode exactly the laminar-flow benefit on which these sections rely (Giguère & Selig, 1997). Third, the angle of attack window stops short of stall, so the stall character of the modified sections, which matters for gust response and for stall-regulated machines, is not established. Fourth, a 5 percent thick section leaves little room for the spar at inboard stations; the structural feasibility of these profiles is plausible at outboard and tip stations but must be verified, and a thicker root section will in practice be blended with them along the span, in the manner of Noronha and Krishna (2020). Fifth, the optimised geometries have not been tested experimentally, a gap this study shares with much of the literature reviewed in Section 2.

Qazi and Sohail studied the factors that affect investors' intention to take part in socially responsible investing. Their research focused on attitude, subjective norms, and perceived behavioral control among Pakistan Stock Exchange investors. The authors highlighted that attitude has a strong role in encouraging socially responsible investment intention.

Mousumi (2026) examined how service quality affects customer engagement and loyalty in Malaysian telecom services. The study showed that improved service quality can increase customer engagement and support long-term customer loyalty. Dr. Nadia Sohail is listed as the supervisor of this study.

5. Conclusion and Future Work

This study set out to optimise the SG6042 airfoil for small horizontal axis wind turbines operating at low Reynolds numbers. The baseline section was analysed in QBlade and its computed behaviour compared with published wind tunnel data, after which eighteen modified geometries, spanning thicknesses of 5 to 9 percent and cambers of 5 to 9 percent of chord, were analysed at Reynolds numbers from 1×10^5 to 6×10^5.

Four conclusions follow. First, every modified geometry outperformed the baseline at every Reynolds number examined, and at Re = 6×10^5 all modified profiles exceeded a lift-to-drag ratio of 160. Second, reduced thickness and raised camber act in the same direction: each percent of added thickness costs about five points of peak efficiency at Re = 5×10^5, while camber raises the peak up to about 8 percent of chord and broadens the efficiency plateau up to 9 percent. Third, the best sections are SG6042M5-7, SG6042M5-8 and SG6042M5-9, with peak lift-to-drag ratios of 178.25, 182.41 and 182.40 at 3.5 degrees and Re = 5×10^5, against 124.10 for the baseline under identical settings, a gain of up to 47 percent. Fourth, the optimal angle of attack falls from 5.5 to 6 degrees at Re = 1×10^5 to 3 to 3.5 degrees at Re = 5×10^5 and above, a band that should guide the twist schedule of any blade built on these sections. Future work should proceed on four fronts. Wind tunnel measurement of the three selected sections at Reynolds numbers from 1×10^5 to 5×10^5 is the first requirement, since the present gains rest on a panel method. Second, RANS computation with a transition-sensitive closure would resolve the laminar separation bubble directly and extend the analysis through stall. Third, the sections should be carried into a blade element momentum design of a complete rotor, with a thicker root section blended inboard, so that the gain in section efficiency can be expressed as a gain in power coefficient and annual energy production. Fourth, the structural and aeroelastic feasibility of 5 percent thick outboard sections, including the pitching moment penalty of high camber, requires quantitative assessment before the profiles are adopted in practice. Subject to these checks, the SG6042M5-7 to SG6042M5-9 family offers a documented, reproducible starting point for the blades of the next generation of small horizontal axis wind turbines intended for low wind speed sites.

References

Alaskari, M., Abdullah, O., & Majeed, M. H. (2019). Analysis of wind turbine using QBlade software. IOP Conference Series: Materials Science and Engineering, 518(3).

Alsahlani, A. A., Al-Saad, M., & Al-Mosallam, M. (2023). A study of impacts of airfoil geometry on the aerodynamic performance at low Reynolds number. International Journal of Mechanical Engineering and Robotics Research, 12(2).

Betz, A. (1966). Introduction to the theory of flow machines. Pergamon Press.

Castelli, M. R., Englaro, A., & Benini, E. (2011). The Darrieus wind turbine: Proposal for a new performance prediction model based on CFD. Energy, 36(8), 4919-4934.

Davari, H. S., et al. (2023). Maximizing the peak lift-to-drag coefficient ratio of airfoils by optimizing the ratio of thickness to the camber of airfoils. Sustainable Earth Review, 3(4), 46-61.

Drela, M. (1989). XFOIL: An analysis and design system for low Reynolds number airfoils. In T. J. Mueller (Ed.), Low Reynolds number aerodynamics (pp. 1-12). Springer.

Giguère, P., & Selig, M. S. (1997). Low Reynolds number airfoils for small horizontal axis wind turbines. Wind Engineering, 21(6), 367-380.

Giguère, P., & Selig, M. S. (1998). New airfoils for small horizontal axis wind turbines. Journal of Solar Energy Engineering, 120(2), 108-114.

Henriques, J. C. C., Marques da Silva, F., Estanqueiro, A. I., & Gato, L. M. C. (2009). Design of a new urban wind turbine airfoil using a pressure-load inverse method. Renewable Energy, 34(12), 2728-2734.

Hossain, S., Raiyan, M. F., Akanda, M. N. U., & Jony, N. H. (2014). A comparative flow analysis of NACA 6409 and NACA 4412 aerofoil. International Journal of Research in Engineering and Technology, 3(10), 342-350.

Jha, S., et al. (2018). Effect of Reynolds number on the aerodynamic performance of NACA 0012 aerofoil. IOP Conference Series: Materials Science and Engineering, 377(1).

Kevadiya, M., & Vaidya, H. A. (2013). 2D analysis of NACA 4412 airfoil. International Journal of Innovative Research in Science, Engineering and Technology, 2(5), 1686-1691.

Khalil, Y., Tenghiri, L., Abdi, F., & Bentamy, A. (2020). Improvement of aerodynamic performance of a small wind turbine. Wind Engineering, 44(1), 21-32.

Leloudas, S. N., et al. (2020). Low Reynolds airfoil family for small horizontal axis wind turbines based on RG15 airfoil. SN Applied Sciences, 2.

Limin, Q., et al. (2011). The investigation of the airfoil for the small wind turbine based on the seagull airfoil. In Proceedings of the Asia-Pacific Power and Energy Engineering Conference (pp. 1-4). IEEE.

Miley, S. J. (1982). A catalog of low Reynolds number airfoil data for wind turbine applications (Report No. RFP-3387, UC-60). Rockwell International.

Noronha, N. P., & Krishna, M. (2020). Design and analysis of micro horizontal axis wind turbine using MATLAB and QBlade. International Journal of Advanced Science and Technology, 29(10S), 8877-8885.

Osei, E. Y., Opoku, R., Sunnu, A. K., & Adaramola, M. S. (2020). Development of high-performance airfoils for application in small wind turbine power generation. Journal of Energy, 2020.

Rasheed, M. A., & Al-Qaisy, A. A. (2008). Experimental investigation of aerodynamic characteristics of NACA 23015 under different angles of attack. Engineering and Technology Journal, 27(2).

Roy, S., Das, B., & Biswas, A. (2021). Influence of camber ratio and thickness ratio on the airfoil performance [Conference paper].

Selig, M. S., & McGranahan, B. D. (2004). Wind tunnel aerodynamic tests of six airfoils for use on small wind turbines. Journal of Solar Energy Engineering, 126(4), 986-1001.

Shah, H., Bhattarai, N., Mathew, S., & Lim, C. M. (2012). Low Reynolds number airfoil for small horizontal axis wind turbine blades [Conference paper].

Shah, H., Mathew, S., & Lim, C. M. (2014). A novel low Reynolds number airfoil design for small horizontal axis wind turbines. Wind Engineering, 38(4), 377-391.

Singh, R. K., & Ahmed, M. R. (2013). Blade design and performance testing of a small wind turbine rotor for low wind speed applications. Renewable Energy, 50, 812-819.

Singh, R. K., Ahmed, M. R., Zullah, M. A., & Lee, Y.-H. (2012). Design of a low Reynolds number airfoil for small horizontal axis wind turbines.

Renewable Energy, 42, 66-76.
Suresh, A., & Rajakumar, S. (2019). Design of small horizontal axis wind turbine for low wind speed rural applications. Materials Today: Proceedings.
Wang, J., et al. (2011). Analysis of aerodynamic performance of wind turbine airfoil under the same relative thickness. Water Resources and Power, 29(9).
Wang, Y., et al. (2018). Investigation on aerodynamic performance of vertical axis wind turbine with different series airfoil shapes. Renewable Energy, 126, 801-818.
Wata, J., Faizal, M., Talu, B., Vanawalu, L., Sotia, P., & Ahmed, M. R. (2011). Studies on a low Reynolds number airfoil for small wind turbine applications. Science China Technological Sciences, 54(7), 1684-1688.
Yang, S. L., Chang, Y. L., & Arici, O. (1995). Navier-Stokes computations of the NREL airfoil using a k-omega turbulent model at high angles of attack. Journal of Solar Energy Engineering, 117(4), 304-310.
Yao, J., et al. (2012). Numerical simulation of aerodynamic performance for two dimensional wind turbine airfoils. Procedia Engineering, 31, 80-86.
Rind, A. A., Luhur, M. R., Manganhar, A. L., Ghoto, S. M., & Bhangwar, S. (2026). Design Optimization of a Low Reynolds Number Airfoil SG6043 for Small Horizontal Axis Wind Turbines. *Wind*, *6*(2), 20.
Qazi, M. A., & Sohail, N. (n.d.). *Factors influencing the intention to engage in socially responsible investing*. *Journal of Economic Innovation and Development*. https://globalscientifichub.com/index.php/JEID
Mousumi, A. (2026). *Service quality, engagement, and loyalty in Malaysian telecom*. *International Journal of Business and Social Science Studies, 6*(1). https://ijbsss.com/index